Received: xxx **Accepted:** xxx **Published:** xxx.
DOI. xxxxxxx
Volume xxx, Issue xxx, p.p. 1-30: xxx
Research Article

Open Access

Control and Optimization in Applied Mathematics - COAM

Analysis and Optimal Control Framework of a Chickenpox Transmission Model with Integrated Vaccination, Isolation-Induced Contact Reduction, Treatment, and Awareness Strategies

Asiyeh Ebrahimzadeh

Department of Mathematics Education, Farhangian University, P.O. Box 14665-889, Tehran, Iran

✉ **Correspondence:**
Asiyeh Ebrahimzadeh
E-mail:
a.ebrahimzadeh@cfu.ac.ir

Abstract. This paper presents a chickenpox-inspired mathematical modeling framework for analyzing varicella-like disease transmission dynamics, using a modified compartmental model that incorporates vaccination, isolation-induced contact reduction, treatment efficacy, and public awareness interventions. The objective is to develop an optimal-control framework and compare scenario-based intervention policies aimed at decreasing infection rates while considering economic and public-health constraints. For scenario comparison, the numerical simulations use fixed representative control levels; they do not numerically solve for time-dependent optimal control trajectories. The research applies Pontryagin's Maximum Principle to formulate a theoretical optimal control framework, including the most critical intervention measures such as vaccination, isolation-induced contact reduction, treatment efficacy, and public awareness. Sensitivity analysis is utilized to examine the impact of model parameters on disease transmission, focusing on the basic reproduction number $\mathcal{R}_0$. Numerical computations under various control regimes reveal that an appropriate combination of vaccination, isolation-induced contact reduction, treatment improvement, and public awareness campaigns can effectively reduce infection rates and provide theoretical insights into community-level intervention planning. The findings are highly beneficial for policymakers by supporting the evaluation of epidemic intervention scenarios and resource allocation decisions in public health administration.

Keywords. Chickenpox (Varicella), Epidemic modeling, Optimal control, Vaccination, Isolation-induced contact reduction, Sensitivity analysis.

MSC. 92D30; 49J15; 34D20.

How to Cite
Ebrahimzadeh, A. (2027). "Analysis and optimal control framework of a chickenpox transmission model with integrated vaccination, isolation-induced contact reduction, treatment, and awareness strategies". *Control and Optimization in Applied Mathematics*, X(x), 1–30. https://doi.org/10.30473/coam.2026.76343.1357

https://mathco.journals.pnu.ac.ir

1 Introduction

Chickenpox (varicella) is a highly contagious viral infection caused by the varicella-zoster virus (VZV), predominantly affecting children and spreading through respiratory droplets and direct contact. Varicella is one of the most contagious human viral infections, and its reported basic reproduction number ($\mathcal{R}_0$) usually ranges between 8 and 10 in unvaccinated populations [17, 21]. Before the implementation of routine varicella vaccination programs, chickenpox imposed a substantial global morbidity burden; although vaccination has significantly reduced disease incidence in countries with high coverage, disparities in immunization policies and coverage continue to contribute to periodic outbreaks worldwide [45]. Recent studies have evaluated the effectiveness of varicella vaccination programs in population-based settings. Barbieri et al. [10] assessed the effectiveness of varicella vaccination among children under the age of 14 in a high-coverage setting and demonstrated a significant reduction in the number of cases after vaccination. Similarly, using surveillance data, Shi et al. [41] reported that varicella immunization programs had a great impact on disease incidence. The dynamics of chickenpox transmission remain relevant to the evaluation of vaccination, isolation, treatment, and awareness measures. Mathematical modeling can therefore be used to assess disease control measures and their possible impacts on epidemics. Such modeling is one of the best ways of understanding the dynamics of disease behavior, predicting future outbreaks, and devising interventions that help reduce mortalities and protect communities [22, 42, 43]. Estimation of epidemiologically critical parameters such as the basic reproduction number ($\mathcal{R}_0$) is one of the foundations of infectious disease modeling, as it helps in gauging the scope of a potential epidemic and identifying appropriate control measures [27].

The mathematical models help in assessing different control measures through disease dynamics simulation. Common mathematical models used in disease modeling include the SIR model, compartmental models, and agent-based models, which are applied to the assessment of vaccinations, quarantines, and treatment [1, 8, 14, 35, 38]. Although compartmental models form the backbone of disease modeling, they rest on a homogeneity assumption that does not account for real-life factors such as spatial heterogeneities and demographic variation [25]. Mathematical models also optimize resource use and shape public health policy, and they play an important role in epidemic forecasting. An additional application of such modeling is the estimation of herd immunity thresholds, which are very useful in the development of vaccination strategies and long-term disease control programs. For decades, epidemic control models have formed the main interest of mathematical epidemiology, growing from simple compartmental models to advanced optimal control models that incorporate vaccinations, quarantines, and healthcare interventions.

The classical SIR epidemic model proposed by Kermack and McKendrick [31] was one of the first and most prominent epidemic models. Recent studies have revisited and extended this

classical framework to address practical limitations such as model–data correspondence, parameter estimation, and the under-reporting of infections [30]. This relatively simple but informative model has since been generalized into more complex compartmental models—such as SEIR and SEIRS—incorporating additional epidemiological features including incubation periods, demographics, and interventions [7, 15, 16, 28, 32]. Some of the latest innovations include network-based models that improve the estimation of the influence of different interventions on disease spread [20]. Mathematical achievements in epidemiology have also contributed to the emergence of age-structured and spatial models that account for heterogeneity in the population structure to describe group-specific transmission dynamics [25]. More recently, Ouakka et al. [39] presented a computational varicella model taking into consideration age-dependent waning immunity and optimal control methods. Adding stochastic elements to epidemic models has provided a basis for modeling variability in disease outbreaks, especially in smaller populations and in cases of unstable disease transmission [15]. In addition, including control measures in epidemic models is an important achievement in epidemiology, where methods such as Pontryagin's Maximum Principle are widely applied to develop optimal vaccination, quarantine, and treatment strategies [34]. The optimal control problem in the context of epidemics has been addressed by formulating objective functions that balance infection reduction and intervention costs under epidemiological and economic constraints [12, 40].

The recent modeling studies focusing specifically on varicella have demonstrated the impact of vaccination programs on disease transmission control. For example, Kim et al. [33] developed an age-structured mathematical model to assess the impact of various vaccination strategies on varicella epidemiology and economics. Similarly, the transmission dynamics of chickenpox were investigated by Nkeki and Mbarie [37], where vaccination, quarantine, and preventive measures were incorporated to control disease transmission.

Several studies have demonstrated the effectiveness of optimal control strategies in slowing disease spread [2, 5, 6, 9, 44]. For instance, Behncke [12] employed optimal control for the SIR model with immunization and demonstrated that time-dependent vaccination policies strongly alter the dynamics of the disease. In the same vein, Blayneh et al. [13] applied control models for vector-borne diseases by introducing insecticide application as a form of control.

Recent studies have also investigated fractional-order epidemic models to capture memory effects and complex transmission dynamics [36]. For example, Akbari et al. [3] developed a fractional-order SEIR model and investigated the local and global stability of its equilibrium points. Within the optimal-control setting, Heydari Dastjerdi et al. [26] applied Pontryagin's principle and artificial neural networks to approximate the state and costate variables and determine a vaccination strategy for an SEIR epidemic model. Despite the advances in epidemic control modeling, several challenges still persist. Among the most significant is accurately capturing human behavioral responses to interventions, which has a substantial effect on the effectiveness of control measures [20]. Subsequent research must examine multi-scale mod-

els incorporating individual-level mixing as well as population-level policies to capture and manage more realistic epidemic dynamics. In conclusion, the field of epidemic control modeling has evolved considerably, from basic compartmental models to advanced optimal control and data-based approaches, and has proven highly useful to policymakers in devising effective intervention strategies.

Several recent research works have addressed control approaches for various infectious diseases. Hassan et al. [23] developed a monkeypox transmission model, incorporating contaminated surfaces, and studied the transmission dynamics using Pontryagin's Maximum Principle. While the current paper adopts a similar framework of compartmental modeling and optimal control analysis, the major difference lies in the choice of disease and the explicit consideration of vaccinations, contact reduction due to isolation, treatment efficacy, and awareness-induced interventions among vaccinated individuals. Moreover, Peter et al. [40] considered an optimal control of monkeypox using a four-control model together with the forward-backward sweep method (FBSM) to find time-dependent optimal controls. The present work, by contrast, develops an optimal control framework theoretically and uses fixed representative control levels to evaluate and compare scenarios rather than computing optimal controls numerically. Furthermore, Khanduzi et al. [32] developed an optimization technique based on numerical collocation for COVID-19 optimal control. Unlike their COVID-19 study, which employed a collocation method combined with a coronavirus optimization algorithm to numerically determine optimal control solutions for a Wuhan case study, the present work develops a chickenpox-based five-compartment framework that explicitly integrates vaccination, isolation-induced contact reduction, treatment improvement, and public awareness. Methodologically, the present study derives the optimality system using Pontryagin's Maximum Principle as a theoretical framework and evaluates fixed representative control levels for scenario comparison rather than numerically computing time-dependent optimal control trajectories.

The main aim of this research is to design a childhood varicella disease model based on chickenpox with different intervention measures for qualitative analysis and regulation of infectious disease transmission. Although existing models provide insights into disease transmission, this paper proposes a modified compartmental model with control parameters to enhance the ability to perform qualitative assessment of intervention policies. The optimal control approach is proposed as a theoretical platform for assessing control strategies. The derived control system and optimality conditions form the mathematical basis for assessing the effects of vaccination, reduced contacts due to isolation, treatment, and awareness. The numerical simulation of various control strategies is performed using the model. It is important to note that chickenpox is distinguished by long-lasting immunity in cases of natural infection. Accordingly, the model does not incorporate fast decay of immunity; instead, the loss of immunity parameters are introduced as small phenomenological terms to describe incomplete immunity, population

heterogeneity, uncertainty of immune status, and loss of vaccine-induced immunity. The major contributions of this work are as follows:

- *Modification of an existing model.* The current investigation extends an existing chickenpox model into a varicella-like childhood viral disease model by expanding its intervention strategy. In addition to vaccination and contact reduction through isolation, two additional controls are introduced: treatment efficacy (u_3) and awareness/herd-immunity promotion (u_4). This modification allows the model to evaluate a wide variety of health intervention policies.
- *Comprehensive mathematical framework.* The model provides an improved system of ODEs to capture the impact of treatment interventions and vaccination policies. Stability of the equilibrium points is analyzed and the basic reproduction number ($\mathcal{R}_0$) is derived under various control strategies.
- *Insights for public health policymakers.* The study provides insight into the effectiveness of control interventions. Through simulation of the control strategies, the most appropriate methods are identified for reducing infection rates, preventing disease-induced mortality, and building population-level immunity.

Through these contributions, this study advances mathematical epidemiology and provides a more realistic model for managing infectious disease transmission.

The remainder of this paper is structured as follows. Section 2 discusses the development of the mathematical model together with the state variables, parameters, and assumptions. Section 3 presents the mathematical analysis of the uncontrolled model, covering non-negativity, boundedness, equilibrium points, the basic reproduction number, stability of the disease-free equilibrium, and sensitivity analysis. Section 4 describes the optimal control strategy, including the controlled model, objective function, adjoint equations, and characterization of the optimal controls. Section 5 contains the numerical simulations under various intervention scenarios. Section 6 presents the conclusions, limitations, and directions for future work.

2 Development of Mathematical Model

This section formulates a deterministic model to investigate the dynamics of disease spread. The total population is categorized into five compartments: susceptible population $H_S(t)$, vaccinated population $H_V(t)$, exposed population $H_E(t)$, infected population $H_I(t)$, and recovered population $H_R(t)$. The susceptible class H_S consists of individuals at risk of infection. The vaccinated class H_V contains individuals who have been vaccinated but do not necessarily have full protection. Exposed individuals are those in the incubation period who are not yet

infectious. The infected class H_I comprises clinically infectious individuals capable of transmitting the disease. The recovered class H_R consists of individuals who are immune to the disease. The natural immunity following chickenpox infection is known to be persistent; the return from the recovered compartment to the susceptible compartment is therefore modeled through the small phenomenological constant ϵ, which reflects waning natural immunity.

It is assumed that new individuals join the susceptible class at a constant recruitment rate Π. Vaccination occurs at rate ϑ with efficacy α. The rate of immunity loss among vaccinated individuals is ω, which is distinct from the waning immunity rate ϵ among naturally immune individuals. Individuals from the exposed class progress to the infectious stage at rate σ; some individuals may instead leave the exposed compartment at rate ϕ before progressing to the infectious stage. The parameter ϕ is introduced as a phenomenological transition representing unsuccessful exposure events, where contact with the pathogen does not establish a successful infection [29, 39]. Natural deaths occur at rate δ across all compartments. Infection transmission takes place through contact with infected individuals at rate β. The recovery rate for individuals in the infected class is η, while disease-induced mortality occurs at rate ρ. Transmission terms involving vaccinated individuals ($H_V H_I$) are multiplied by $(1-\alpha)$ to account for partial vaccine protection. The details of all compartments, parameters, and control variables are collected in Table 1.

The dynamics of the infectious disease model without control are described by the following system of ordinary differential equations:

$$\frac{dH_S}{dt} = \Pi - \beta H_S H_I - (\vartheta + \delta) H_S + \omega H_V + \epsilon H_R + \phi H_E, \tag{1}$$

$$\frac{dH_V}{dt} = \vartheta H_S - (1-\alpha)\beta H_V H_I - (\omega + \delta) H_V, \tag{2}$$

$$\frac{dH_E}{dt} = \beta H_S H_I + (1-\alpha)\beta H_V H_I - (\sigma + \phi + \delta) H_E, \tag{3}$$

$$\frac{dH_I}{dt} = \sigma H_E - (\eta + \rho + \delta) H_I, \tag{4}$$

$$\frac{dH_R}{dt} = \eta H_I - (\epsilon + \delta) H_R. \tag{5}$$

The epidemiological parameters are based on previous chickenpox transmission models. Specifically, Jose et al. [29] provided biologically realistic parameter values for the exposed, infectious, and recovery phases. The parameters σ and η reflect the varicella-zoster virus incubation and infection periods, consistent with observed epidemiological features [24]. The waning immunity parameters ϵ and ω are based on previous varicella models that considered incomplete or vaccine-induced immunity loss over time [17, 39]. The control-oriented parameters are introduced in Section 4 as scenario-driven coefficients for qualitative intervention analysis. All parameter values are listed in Table 1.

Table 1: Model parameters, control variables, and initial values of state variables.

Symbol	Description	Value
Π	Recruitment rate (birth or migration)	9
β	Disease transmission rate	1.76×10^{-8}
ω	Immunity loss rate in vaccinated individuals	0.03423
ϕ	Rate at which exposed individuals revert to susceptible state	0.157
δ	Natural death rate	0.00001694
ϑ	Vaccination rate	0.000504
α	Vaccine efficacy	0.0684
ϵ	Immunity waning rate in recovered individuals	0.000429
σ	Rate of progression from exposed to infected state	0.00242
η	Recovery rate of infected individuals	0.002105
ρ	Disease-induced mortality rate	0.00001694
	Control Variables	
u_1	Vaccination control	$[0, 1]$
u_2	Isolation-induced contact-reduction control	$[0, 1]$
u_3	Treatment-efficacy control	$[0, 1]$
u_4	Awareness and herd-immunity promotion	$[0, 1]$
	Initial Values of State Variables	
$H_S(0)$	Initial susceptible population	83 812
$H_V(0)$	Initial vaccinated population	573
$H_E(0)$	Initial exposed population	604
$H_I(0)$	Initial infected population	534
$H_R(0)$	Initial recovered population	178

Furthermore, future research could build on the present model by incorporating age structure, breakthrough infections among vaccinated individuals, time-varying contact rates, and behavioral factors such as vaccine hesitancy and adherence to isolation.

3 Mathematical Analysis of the Modified Chickenpox Model

This section carries out the mathematical analysis of the modified chickenpox model to establish its inherent properties. We first prove the non-negativity and boundedness of solutions to ensure the biological viability of the model. We then compute the equilibrium points and the basic reproduction number, and study the stability of the equilibria.

3.1 Non-Negativity and Boundedness of Solutions

Proposition 1. *The non-negative orthant $\mathbb{R}^5_{\geq 0}$ is positively invariant with respect to system (1)–(5). Moreover, there exists a positive number L such that the compact set*

$$B_u = \left\{(H_S, H_V, H_E, H_I, H_R) \in \mathbb{R}^5_{\geq 0} : 0 \leq H_S, H_V, H_E, H_I, H_R \leq L\right\}$$

is positively invariant.

Proof. From the non-negativity of all of

$$H_S(t),\ H_V(t),\ H_E(t),\ H_I(t),\ H_R(t) \geq 0, \qquad \forall\, t \geq 0,$$

we show boundedness by defining the total population as

$$N(t) = H_S(t) + H_V(t) + H_E(t) + H_I(t) + H_R(t).$$

Summing all equations of system (1)–(5) gives

$$\frac{dN}{dt} = \Pi - \delta N - \rho H_I.$$

Since $\rho H_I \geq 0$, it follows that

$$\frac{dN}{dt} \leq \Pi - \delta N.$$

Comparing with the linear differential equation $\frac{dM}{dt} = \Pi - \delta M$, one obtains

$$N(t) \leq \max\left\{N(0),\ \frac{\Pi}{\delta}\right\}.$$

Hence, the set B_u is positively invariant and the solutions of the model are always non-negative and bounded for all $t \geq 0$. □

3.2 Disease-Free Equilibrium

The disease-free equilibrium (DFE) is derived by setting $H_E = 0$ and $H_I = 0$. Setting the right-hand sides of Equations (1)–(5) to zero gives:

$$\Pi - (\vartheta + \delta)\, H_S + \omega H_V + \epsilon H_R = 0, \tag{6}$$

$$\vartheta H_S - (\omega + \delta)\, H_V = 0, \tag{7}$$

$$-(\epsilon + \delta)\, H_R = 0. \tag{8}$$

From Equation (8) it follows immediately that $H_R = 0$. Substituting $H_R = 0$ into Equations (6) and (7) gives the system

$$\Pi - (\vartheta + \delta)\, H_S + \omega H_V = 0, \tag{9}$$

$$\vartheta H_S - (\omega + \delta)\, H_V = 0. \tag{10}$$

From Equation (10) it follows that

$$H_V = \frac{\vartheta}{\omega + \delta} H_S. \tag{11}$$

Substituting Equation (11) into Equation (9) and solving for H_S yields the susceptible population at equilibrium, along with

$$H_V^0 = \frac{\Pi\vartheta}{\delta(\vartheta + \omega + \delta)}.$$

Therefore, the disease-free equilibrium point is

$$\mathcal{E}_0 = \left(\frac{\Pi(\omega + \delta)}{\delta(\vartheta + \omega + \delta)},\ \frac{\Pi\vartheta}{\delta(\vartheta + \omega + \delta)},\ 0,\ 0,\ 0 \right). \tag{12}$$

For any positive values of the biological parameters we have $H_S^0 > 0$ and $H_V^0 > 0$, ensuring the biological validity of the model at equilibrium.

3.3 Basic Reproduction Number

To compute the basic reproduction number $\mathcal{R}_0$, we employ the next-generation matrix approach [11, 18]. Defining the infected-compartment state vector as $Y = (H_E, H_I)^T$, the dynamics of the infected compartments are written as $\frac{dY}{dt} = \mathcal{F}(Y) - \mathcal{V}(Y)$, where

$$\mathcal{F}(Y) = \begin{bmatrix} \beta H_S H_I + (1-\alpha)\beta H_V H_I \\ 0 \end{bmatrix}, \quad \mathcal{V}(Y) = \begin{bmatrix} (\sigma + \phi + \delta)\, H_E \\ (\eta + \rho + \delta)\, H_I - \sigma H_E \end{bmatrix}.$$

The Jacobian matrices $\bar{F}$ and $\bar{V}$ evaluated at the DFE $\mathcal{E}_0$ given in Equation (12) are

$$\bar{F} = \begin{bmatrix} 0 & \beta H_S^0 + (1-\alpha)\beta H_V^0 \\ 0 & 0 \end{bmatrix}, \quad \bar{V} = \begin{bmatrix} \sigma + \phi + \delta & 0 \\ -\sigma & \eta + \rho + \delta \end{bmatrix}.$$

The inverse of $\bar{V}$ is

$$\bar{V}^{-1} = \frac{1}{(\sigma + \phi + \delta)(\eta + \rho + \delta)} \begin{bmatrix} \eta + \rho + \delta & 0 \\ \sigma & \sigma + \phi + \delta \end{bmatrix}.$$

The next-generation matrix $\mathcal{K} = \bar{F}\bar{V}^{-1}$ has spectral radius

$$\mathcal{R}_0 = \rho(\mathcal{K}) = \frac{\beta\sigma(H_S^0 + (1-\alpha)H_V^0)}{(\sigma + \phi + \delta)(\eta + \rho + \delta)}. \tag{13}$$

Substituting the explicit DFE coordinates into Equation (13) gives

$$\mathcal{R}_0 = \frac{\beta\sigma\Pi\big(\omega + \delta + \vartheta(1-\alpha)\big)}{\delta(\vartheta + \omega + \delta)(\sigma + \phi + \delta)(\eta + \rho + \delta)}. \tag{14}$$

The quantity $\mathcal{R}_0$ denotes the average number of secondary infections generated by a single infected individual in a wholly susceptible population at the DFE. When $\mathcal{R}_0 < 1$, the disease-free equilibrium $\mathcal{E}_0$ is locally asymptotically stable and the disease is eventually eradicated from the population.

3.4 Endemic Equilibrium

The endemic equilibrium E^* refers to the state in which the disease persists in the population, with $H_E^* > 0$ and $H_I^* > 0$. Setting the right-hand sides of system (1)–(5) to zero gives

$$\begin{cases} \Pi - \beta H_S H_I + \omega H_V + \phi H_E - (\delta + \vartheta)\, H_S + \epsilon H_R = 0, \\ \vartheta H_S - (1-\alpha)\beta H_V H_I - (\omega + \delta)\, H_V = 0, \\ (1-\alpha)\beta H_V H_I + \beta H_S H_I - (\sigma + \delta + \phi)\, H_E = 0, \\ \sigma H_E - (\eta + \delta + \rho)\, H_I = 0, \\ \eta H_I - (\delta + \epsilon)\, H_R = 0. \end{cases} \tag{15}$$

Introducing the auxiliary parameters

$$\begin{aligned} c_1 &= \beta, & c_2 &= \delta + \vartheta, & c_3 &= \vartheta, \\ c_4 &= (1-\alpha)\beta, & c_5 &= \omega + \delta, & c_6 &= \sigma + \delta + \phi, \\ c_7 &= \eta + \delta + \rho, & c_8 &= \eta, & c_9 &= \delta + \epsilon, \end{aligned}$$

the equilibrium values of the state variables as functions of H_E^* are

$$\begin{cases} H_I^* = \dfrac{\sigma H_E^*}{c_7}, \\ H_R^* = \dfrac{c_8 \sigma H_E^*}{c_7 c_9}, \\ H_V^* = \dfrac{c_3 H_S^*}{c_4 \dfrac{\sigma H_E^*}{c_7} + c_5}, \\ H_S^* = \dfrac{\Pi + \omega H_V^* + (\phi - c_6) H_E^* + \epsilon H_R^*}{c_2}. \end{cases} \tag{16}$$

Substituting the expressions in Equation (16) into the third equation of system (15) yields the quadratic equation

$$\bar{A} (H_E^*)^2 + \bar{B} H_E^* + \bar{C} = 0, \tag{17}$$

whose coefficients $\bar{A}$, $\bar{B}$, and $\bar{C}$ are functions of the model parameters. When $\mathcal{R}_0 > 1$, we have $\bar{C} < 0$, guaranteeing a unique positive root

$$H_E^* = \frac{-\bar{B} + \sqrt{\bar{B}^2 - 4\bar{A}\bar{C}}}{2\bar{A}}.$$

It then follows from Equation (16) that all state variables $H_S^*, H_V^*, H_I^*, H_R^*$ are positive at the endemic equilibrium E^*.

3.5 Local Stability of the Disease-Free Equilibrium

The Jacobian matrix evaluated at the DFE $\mathcal{E}_0 = (H_S^0, H_V^0, 0, 0, 0)$ takes the form

$$J(\mathcal{E}_0) = \begin{pmatrix} -(\delta + \vartheta) & \omega & \phi & -\beta H_S^0 & \epsilon \\ \vartheta & -(\omega + \delta) & 0 & -(1-\alpha)\beta H_V^0 & 0 \\ 0 & 0 & -(\sigma + \delta + \phi) & \beta H_S^0 + (1-\alpha)\beta H_V^0 & 0 \\ 0 & 0 & \sigma & -(\eta + \delta + \rho) & 0 \\ 0 & 0 & 0 & \eta & -(\delta + \epsilon) \end{pmatrix}.$$

One eigenvalue is obtained directly from the triangular structure:

$$\lambda_1 = -(\delta + \epsilon) < 0.$$

The remaining eigenvalues are determined by the upper-left 4×4 block and are governed by the infection dynamics. The DFE exhibits the standard threshold behavior: the DFE is locally asymptotically stable if $\mathcal{R}_0 < 1$, and unstable if $\mathcal{R}_0 > 1$. Substituting the baseline parameter values from Table 1 into Equation (14) yields $\mathcal{R}_0 = 0.0663 < 1$. The numerically computed eigenvalues of $J(\mathcal{E}_0)$ are presented in Table 2; all satisfy $\mathrm{Re}(\lambda_i) < 0$, confirming local asymptotic stability.

Table 2: Eigenvalues of the Jacobian matrix at the disease-free equilibrium for $\mathcal{R}_0 < 1$.

Equilibrium	Eigenvalues (λ_i)	Stability status
Disease-free equilibrium ($\mathcal{E}_0$)	$\lambda_1 \approx -0.1594, \quad \lambda_2 \approx -0.0347,$ $\lambda_3 \approx -0.0021, \quad \lambda_4 \approx -4.45 \times 10^{-4},$ $\lambda_5 \approx -1.69 \times 10^{-5}$	Locally asymptotically stable

From an epidemiological perspective, small perturbations from the DFE lead to extinction of the disease. If $\mathcal{R}_0 > 1$, the DFE becomes unstable and the system admits a unique endemic equilibrium $E^* = (H_S^*, H_V^*, H_E^*, H_I^*, H_R^*)$ with all coordinates positive, representing persistent disease in the population. Since the main aim of this study is to apply the optimal control framework to drive the system to the DFE, the stability analysis is focused on $\mathcal{E}_0$. With the baseline parameter values from Table 1, the reproduction number is $\mathcal{R}_0 = 0.0663 < 1$, ensuring local asymptotic stability of the DFE.

3.6 Sensitivity Analysis of $\mathcal{R}_0$

Sensitivity analysis is important for determining the parameters that most significantly influence chickenpox transmission. The normalized forward sensitivity index (elasticity) of $\mathcal{R}_0$ with respect to a parameter θ is defined as

$$S_\theta^{\mathcal{R}_0} = \frac{\partial \mathcal{R}_0}{\partial \theta} \times \frac{\theta}{\mathcal{R}_0}.$$

The indices are computed at the baseline parameter values in Table 1, at which $\mathcal{R}_0 \approx 0.0663$ from Equation (14). As examples, the partial derivatives with respect to β and ϕ are computed. Because β appears linearly in the numerator of Equation (14), its partial derivative gives $S_\beta^{\mathcal{R}_0} = 1$, showing a direct proportional relationship between the transmission rate and $\mathcal{R}_0$. For ϕ, one obtains

$$S_\phi^{\mathcal{R}_0} = -\frac{\phi}{\sigma + \phi + \delta},$$

indicating that increasing ϕ decreases $\mathcal{R}_0$. The computed sensitivity indices are summarized in Table 3. These represent the percentage change in $\mathcal{R}_0$ for a 1% increase in the corresponding parameter.

As shown in Table 3, $\mathcal{R}_0$ is most sensitive to the transmission rate (β) and the recruitment rate (Π), both with a sensitivity index of $+1.00$, meaning a 10% increase in either parameter leads to a 10% increase in $\mathcal{R}_0$. The exposed-to-susceptible transition rate (ϕ) and the recovery rate (η) exhibit significant negative sensitivity, confirming that increasing these rates is the most effective means of reducing disease burden and achieving elimination.

Table 3: Normalized forward sensitivity indices of $\mathcal{R}_0$ for the chickenpox model evaluated at the baseline parameter values in Table 1 ($\mathcal{R}_0 \approx 0.0663$).

Parameter	Symbol	Sensitivity index
Transmission rate	β	$+1.0000$
Recruitment rate	Π	$+1.0000$
Progression rate (exposed to infected)	σ	$+0.9848$
Immunity-waning rate	ω	$+0.0010$
Exposed-to-susceptible transition rate	ϕ	-0.9837
Natural death rate	δ	-1.0070
Recovery rate	η	-0.9832
Vaccine efficacy	α	-0.0010
Disease-induced mortality rate	ρ	-0.0079

4 Optimal Control and Intervention Policies

The method of optimal control is significant for formulating appropriate strategies to reduce the spread of infection. By formulating the optimal control problem, we aim to minimize the cost associated with both the infection itself and the cost of the interventions.

4.1 Introduction of Control Variables

In mathematical epidemiology, adding control variables to disease transmission models is an effective way of optimizing intervention policies and reducing disease spread. Four control variables are introduced, addressing the key areas of preventing infection, improving treatment, and promoting health awareness.

The first control variable, $u_1(t)$, represents the vaccination effort. An increase in $u_1(t)$ increases the number of vaccinated individuals and thereby decreases the infection transmission rate. The second control variable, $u_2(t)$, represents isolation-induced contact reduction. For chickenpox-like infections, isolation primarily reduces effective contacts between infectious and susceptible individuals. The third control variable, $u_3(t)$, represents treatment efficacy. A larger $u_3(t)$ accelerates recovery and shortens the infectious period. The fourth control variable, $u_4(t)$, represents public health awareness and education campaigns that create public awareness and promote vaccination.

These control measures constitute a coherent disease control policy encompassing vaccination, quarantine, treatment, and public education. We will formulate the objective function

and the control constraints, then utilize Pontryagin's Maximum Principle to derive the optimal intervention model in Subsection 4.3.

4.2 Objective Function and Control Constraints

The objective of the optimal control problem is to minimize the total cost incurred through disease transmission and the implementation of control strategies. The cost functional is

$$J = \int_0^T \left[A_1 H_I(t) + A_2 u_1^2(t) + A_3 u_2^2(t) + A_4 u_3^2(t) + A_5 u_4^2(t) \right] dt, \tag{18}$$

where T is the final intervention time, A_1 represents the socioeconomic burden of the disease, and A_i $(i = 2, 3, 4, 5)$ represent the relative costs associated with each control measure. The quadratic control terms discourage overly intensive interventions by imposing extra costs, leading to more balanced and cost-efficient strategies. The control functions are bounded:

$$0 \leq u_i(t) \leq 1, \qquad i = 1, 2, 3, 4,$$

where $u_i(t) = 0$ indicates no intervention and $u_i(t) = 1$ indicates maximum intervention effort.

For dimensional consistency, the efficiency parameters κ_1, κ_3, and κ_4 (all in units of day^{-1}) are introduced as described in Table 4. The control functions $u_1(t)$, $u_3(t)$, and $u_4(t)$ are dimensionless, with effective intervention rates $\kappa_1 u_1(t)$, $\kappa_3 u_3(t)$, and $\kappa_4 u_4(t)$ (day^{-1}) appearing in the state equations.

Table 4: Description and ranges of the control-efficiency parameters.

Symbol	Description	Unit	Range
κ_1	Maximum vaccination-control efficiency	day^{-1}	[0, 0.5]
κ_3	Maximum treatment-induced recovery efficiency	day^{-1}	[0, 0.2]
κ_4	Maximum awareness-induced vaccination efficiency	day^{-1}	[0, 0.1]

Incorporating the four control functions into the uncontrolled baseline system (1)–(5) yields the controlled epidemic model:

$$\frac{dH_S}{dt} = \Pi - (1-u_2)\beta H_S H_I - (\vartheta + \kappa_1 u_1 + \kappa_4 u_4 + \delta) H_S + \omega H_V + \epsilon H_R + \phi H_E, \tag{19}$$

$$\frac{dH_V}{dt} = (\vartheta + \kappa_1 u_1 + \kappa_4 u_4) H_S - (1-u_2)(1-\alpha)\beta H_V H_I - (\omega + \delta) H_V, \tag{20}$$

$$\frac{dH_E}{dt} = (1-u_2)\beta H_S H_I + (1-u_2)(1-\alpha)\beta H_V H_I - (\sigma + \phi + \delta) H_E, \tag{21}$$

$$\frac{dH_I}{dt} = \sigma H_E - (\eta + \kappa_3 u_3 + \rho + \delta)\, H_I, \tag{22}$$

$$\frac{dH_R}{dt} = (\eta + \kappa_3 u_3)\, H_I - (\epsilon + \delta)\, H_R. \tag{23}$$

Control u_1 directly increases the transition rate from H_S to H_V. Control u_2 limits contacts between infectious and susceptible individuals through the factor $(1-u_2)$. Control u_3 increases the recovery rate of infected individuals. Control u_4 promotes vaccination among susceptibles through awareness-induced immunization.

The optimal control problem consists in finding the control functions $(u_1^*(t), u_2^*(t), u_3^*(t), u_4^*(t))$ that minimize the cost functional J in Equation (18). In Subsection 4.3, Pontryagin's Maximum Principle is used to derive the necessary optimality conditions and characterize the optimal control functions.

4.3 Application of Pontryagin's Maximum Principle

Pontryagin's Maximum Principle (PMP) converts the optimal control problem into a set of state equations, adjoint equations, and optimality conditions. The state vector and adjoint vector are

$$X(t) = \big(H_S(t), H_V(t), H_E(t), H_I(t), H_R(t)\big)^T,$$
$$\lambda(t) = \big(\lambda_1(t), \lambda_2(t), \lambda_3(t), \lambda_4(t), \lambda_5(t)\big)^T.$$

The Hamiltonian function associated with system (19)–(23) and cost functional (18) is

$$\begin{aligned}
\mathcal{H} = {} & A_1 H_I + A_2 u_1^2 + A_3 u_2^2 + A_4 u_3^2 + A_5 u_4^2 \\
& + \lambda_1 \Big[\Pi - (1-u_2)\beta H_S H_I - (\vartheta + \kappa_1 u_1 + \kappa_4 u_4 + \delta)\, H_S + \omega H_V + \epsilon H_R + \phi H_E\Big] \\
& + \lambda_2 \Big[(\vartheta + \kappa_1 u_1 + \kappa_4 u_4)\, H_S - (1-u_2)(1-\alpha)\beta H_V H_I - (\omega + \delta)\, H_V\Big] \\
& + \lambda_3 \Big[(1-u_2)\beta H_S H_I + (1-u_2)(1-\alpha)\beta H_V H_I - (\sigma + \phi + \delta)\, H_E\Big] \\
& + \lambda_4 \Big[\sigma H_E - (\eta + \kappa_3 u_3 + \rho + \delta)\, H_I\Big] + \lambda_5 \Big[(\eta + \kappa_3 u_3)\, H_I - (\epsilon + \delta)\, H_R\Big].
\end{aligned}$$

By PMP, the adjoint equations satisfy $\dot{\lambda}_i(t) = -\partial \mathcal{H}/\partial x_i$, giving

$$\begin{aligned}
\dot{\lambda}_1 &= \lambda_1 \Big[(1-u_2)\beta H_I + \vartheta + \kappa_1 u_1 + \kappa_4 u_4 + \delta\Big] - \lambda_2(\vartheta + \kappa_1 u_1 + \kappa_4 u_4) - \lambda_3(1-u_2)\beta H_I, \\
\dot{\lambda}_2 &= -\lambda_1 \omega + \lambda_2 \Big[(1-u_2)(1-\alpha)\beta H_I + \omega + \delta\Big] - \lambda_3(1-u_2)(1-\alpha)\beta H_I, \\
\dot{\lambda}_3 &= -\lambda_1 \phi + \lambda_3(\sigma + \phi + \delta) - \lambda_4 \sigma, \\
\dot{\lambda}_4 &= -A_1 + \lambda_1(1-u_2)\beta H_S + \lambda_2(1-u_2)(1-\alpha)\beta H_V \\
&\quad - \lambda_3 \Big[(1-u_2)\beta H_S + (1-u_2)(1-\alpha)\beta H_V\Big] + \lambda_4(\eta + \kappa_3 u_3 + \rho + \delta) - \lambda_5(\eta + \kappa_3 u_3),
\end{aligned}$$

$\dot{\lambda}_5 = -\lambda_1\epsilon + \lambda_5(\epsilon + \delta)$.

The transversality conditions are

$$\lambda_1(T) = \lambda_2(T) = \lambda_3(T) = \lambda_4(T) = \lambda_5(T) = 0.$$

From the stationary conditions $\partial\mathcal{H}/\partial u_i = 0$ $(i = 1, 2, 3, 4)$, and applying the constraints $0 \leq u_i(t) \leq 1$, the optimal control functions are characterized as

$$u_1^*(t) = \max\left\{0, \min\left(1, \frac{\kappa_1 H_S(\lambda_1 - \lambda_2)}{2A_2}\right)\right\}, \tag{24}$$

$$u_2^*(t) = \max\left\{0, \min\left(1, \frac{\beta H_I\left[H_S(\lambda_1 - \lambda_3) + (1-\alpha)H_V(\lambda_2 - \lambda_3)\right]}{2A_3}\right)\right\}, \tag{25}$$

$$u_3^*(t) = \max\left\{0, \min\left(1, \frac{\kappa_3 H_I(\lambda_4 - \lambda_5)}{2A_4}\right)\right\}, \tag{26}$$

$$u_4^*(t) = \max\left\{0, \min\left(1, \frac{\kappa_4 H_S(\lambda_1 - \lambda_2)}{2A_5}\right)\right\}. \tag{27}$$

The optimality system comprises the state equations (19)–(23), the adjoint equations, the transversality conditions, and the optimal control characterizations (24)–(27). This two-point boundary value problem can be solved numerically using the forward-backward sweep procedure described in Subsection 4.4.

4.4 Forward-Backward Sweep Procedure

The optimality system derived in Subsection 4.3 can be solved numerically using the forward-backward sweep method (FBSM). The state variables are subject to initial conditions while the adjoint variables satisfy terminal conditions, making the system a two-point boundary value problem. The iterative procedure is as follows:

1. Select initial control approximations $u_i^{(0)}(t)$ on $[0, T]$ $(i = 1, 2, 3, 4)$, and choose a tolerance $\varepsilon_{\text{tol}} > 0$. Set $n = 0$.
2. Using the current controls $u_i^{(n)}(t)$, integrate the state system (19)–(23) forward in time from $t = 0$ to $t = T$ under the specified initial conditions.
3. Integrate the adjoint equations backward from $t = T$ to $t = 0$, imposing the transversality conditions $\lambda_i(T) = 0$, $i = 1, \ldots, 5$.
4. Update the control variables point-wise using the characterizations (24)–(27): $u_i^{(n+1)}(t)$, $i = 1, 2, 3, 4$.

5. Apply the relaxation update for numerical stability:

$$u_i^{(n+1)}(t) = \theta\, u_i^{(n+1)}(t) + (1-\theta)\, u_i^{(n)}(t), \qquad 0 < \theta \leq 1, \quad i = 1, 2, 3, 4.$$

6. Evaluate the iteration error $E = \max_{t\in[0,T]} \max_{1\leq i\leq 4} \left| u_i^{(n+1)}(t) - u_i^{(n)}(t) \right|$. If $E < \varepsilon_{\text{tol}}$, stop; otherwise set $n \leftarrow n+1$ and return to Step 2.

The FBSM algorithm enables the computation of time-dependent optimal control strategies from the optimality system. In the present work, the focus is on the mathematical derivation of the optimal control problem, while the scenario simulations in Section 5 demonstrate the comparative effects of different fixed-level intervention combinations.

5 Numerical Simulations under Different Scenarios

To illustrate the applicability of the optimal control framework proposed in the preceding sections, five fixed control scenarios are considered. These scenarios represent different intervention intensities within the optimal control framework and are designed to provide comparative insights into the effectiveness of vaccination, isolation-induced contact reduction, treatment, and awareness strategies. The controlled state system is numerically integrated over $[0, T]$ using the standard fourth-order Runge–Kutta algorithm with constant time step size Δt.

The same baseline parameters from Table 1 are used in all scenarios to ensure comparability. Robustness of the numerical scheme was validated by repeating simulations with smaller time steps. The control parameters were chosen within the normalized range $[0, 1]$; smaller values correspond to weaker public health intervention efforts. The chosen controls are intended for comparative analysis of intervention policies, not for calibration purposes. The epidemiological parameter values are taken from the baseline study [4].

5.1 Strategy 1: Minimal Intervention (Baseline Strategy)

This strategy represents a scenario of low intervention that serves as the baseline against which other strategies are compared. The control variables are set to $u_1 = 0.2$, $u_2 = 0.1$, $u_3 = 0.1$, and $u_4 = 0.1$.

Figure 1 presents the disease dynamics under weak control effort. Compared to the uncontrolled model, the controlled model shows a decrease in the number of infected individuals and an increase in the number of recovered individuals. The susceptible population also decreases due to vaccination and awareness efforts, although these are minimal. These results suggest that even minimal intervention can help lower disease spread, but stronger strategies are needed.

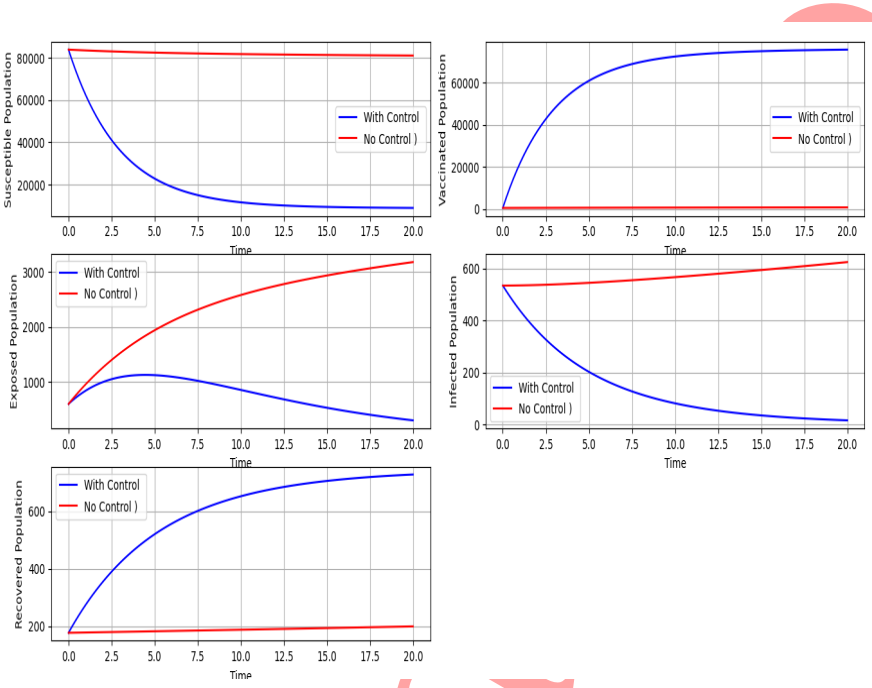

Figure 1: Comparison between the dynamics of the disease model with and without controls under Strategy 1 ($u_1 = 0.2, u_2 = 0.1, u_3 = 0.1, u_4 = 0.1$).

5.2 Strategy 2: Aggressive Vaccination and Awareness Campaigns

This approach focuses on high vaccination levels combined with vigorous awareness campaigns to decrease the susceptible population rapidly. The control variables are set to $u_1 = 0.9$, $u_2 = 0.1$, $u_3 = 0.4$, and $u_4 = 0.9$.

Figure 2 shows the impact of intensive vaccination and awareness programs. The number of susceptibles reduces dramatically, and there is a corresponding increase in the number of vaccinated individuals. Infected individuals decrease drastically, indicating that the strategy is very effective in controlling the transmission rate. A slight initial rise in exposed individuals due to residual transmission is followed by a decline. The number of recovered individuals consistently increases. In general, this approach is very effective when there is an urgent need to suppress an epidemic.

5.3 Strategy 3: Strict Isolation and Quarantine

The third strategy focuses mainly on isolation and quarantine policies to minimize effective contacts between infectious and susceptible individuals. The control variables are set to $u_1 = 0.3$, $u_2 = 0.9$, $u_3 = 0.8$, and $u_4 = 0.3$.

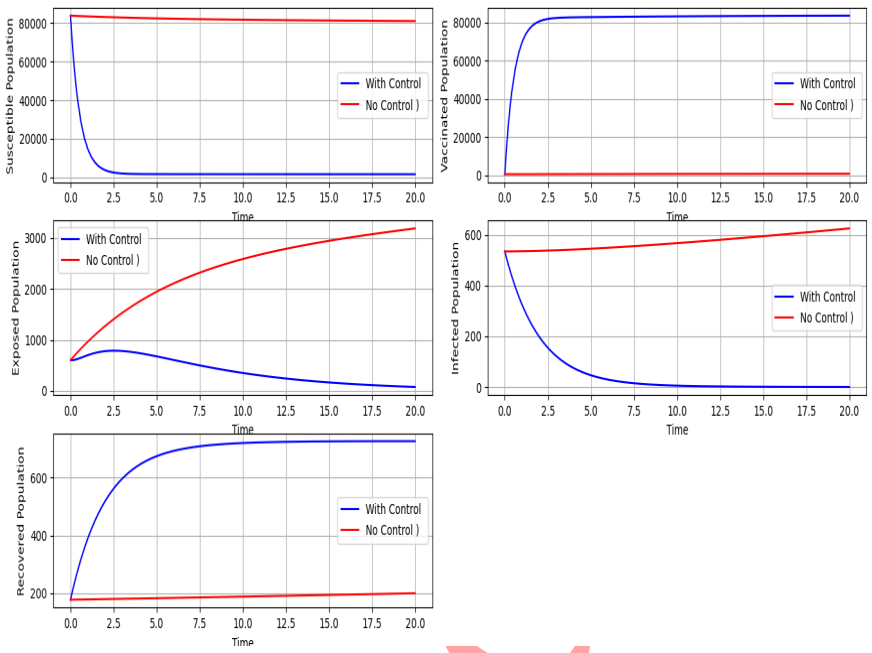

Figure 2: Comparison of model dynamics with and without control measures under Strategy 2 ($u_1 = 0.9$, $u_2 = 0.1$, $u_3 = 0.4$, $u_4 = 0.9$).

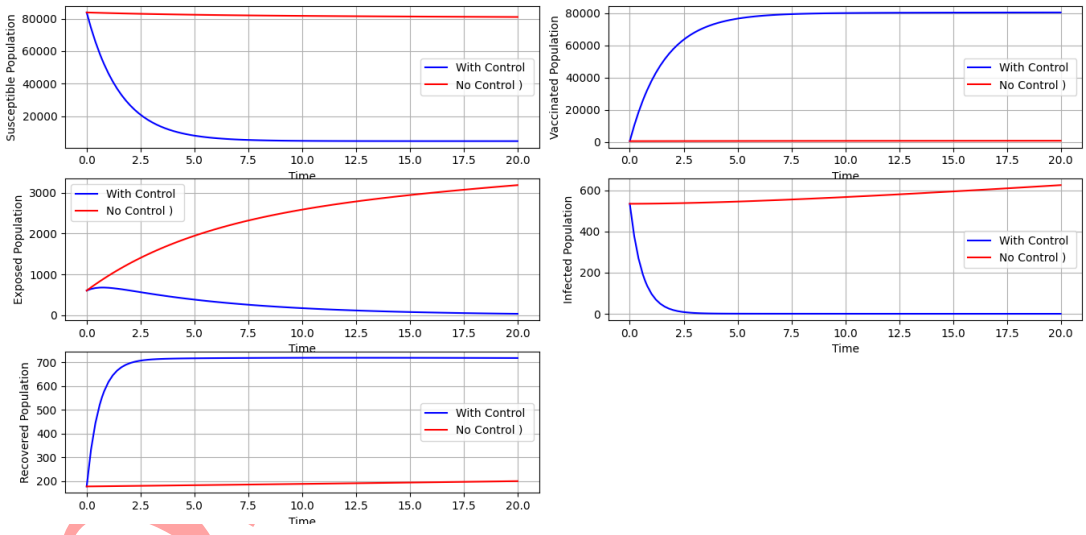

Figure 3: Dynamics comparison of the disease model with and without control measures under Strategy 3 ($u_1 = 0.3$, $u_2 = 0.9$, $u_3 = 0.8$, $u_4 = 0.3$).

Figure 3 presents the impact of effective isolation and quarantine combined with moderate vaccination and treatment. The number of infected individuals decreases substantially due to reduced contacts. The exposed population does not become large, while the recovered population grows.

5.4 Strategy 4: Increased Treatment and Herd-Immunity Promotion

This strategy combines increased treatment efficiency with herd-immunity awareness to decrease infection prevalence and increase recovery. The control variables are set to $u_1 = 0.5$, $u_2 = 0.3$, $u_3 = 0.9$, and $u_4 = 0.7$.

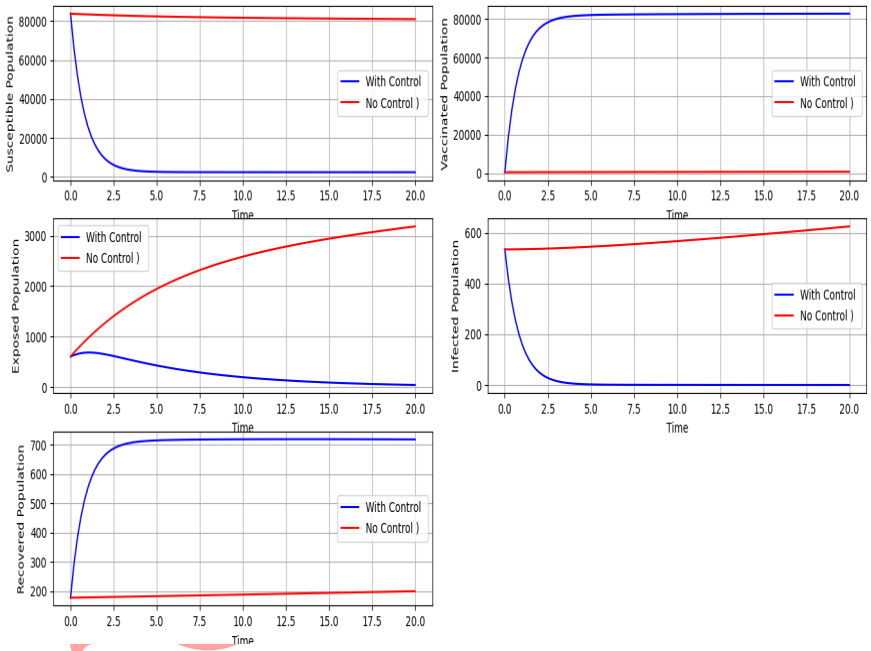

Figure 4: Dynamics comparison of disease models with and without control measures under Strategy 4 ($u_1 = 0.5$, $u_2 = 0.3$, $u_3 = 0.9$, $u_4 = 0.7$).

Figure 4 shows that an improved treatment rate combined with a public awareness program results in a decrease in infected individuals and an increase in recovered individuals. The susceptible population falls gradually while the vaccinated population grows. The exposed population first increases then decreases, demonstrating the vital role of treatment enhancement and public health awareness in combating the epidemic.

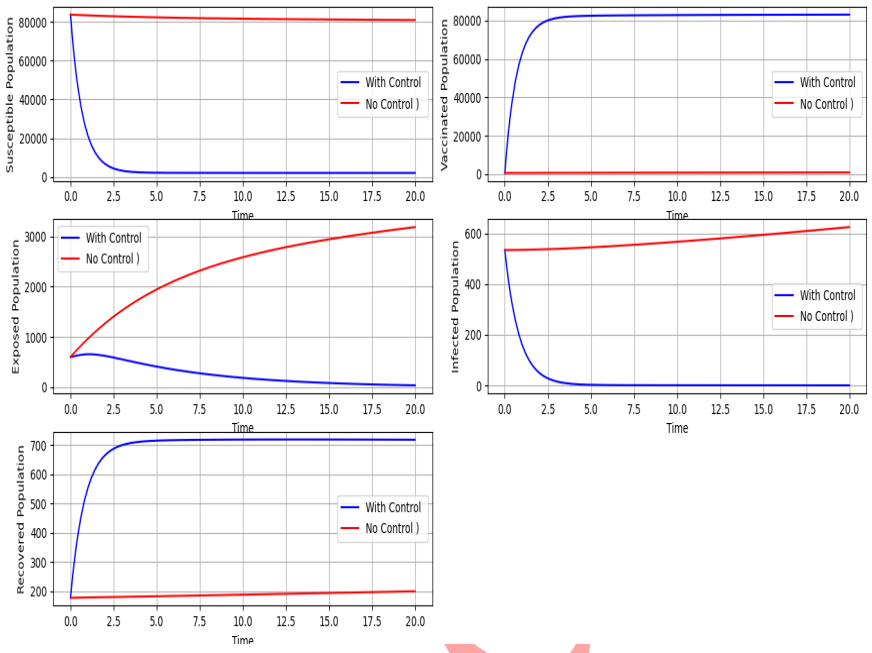

Figure 5: Comparison of disease model dynamics with and without controls under Strategy 5 ($u_1 = 0.7, u_2 = 0.5, u_3 = 0.7, u_4 = 0.7$).

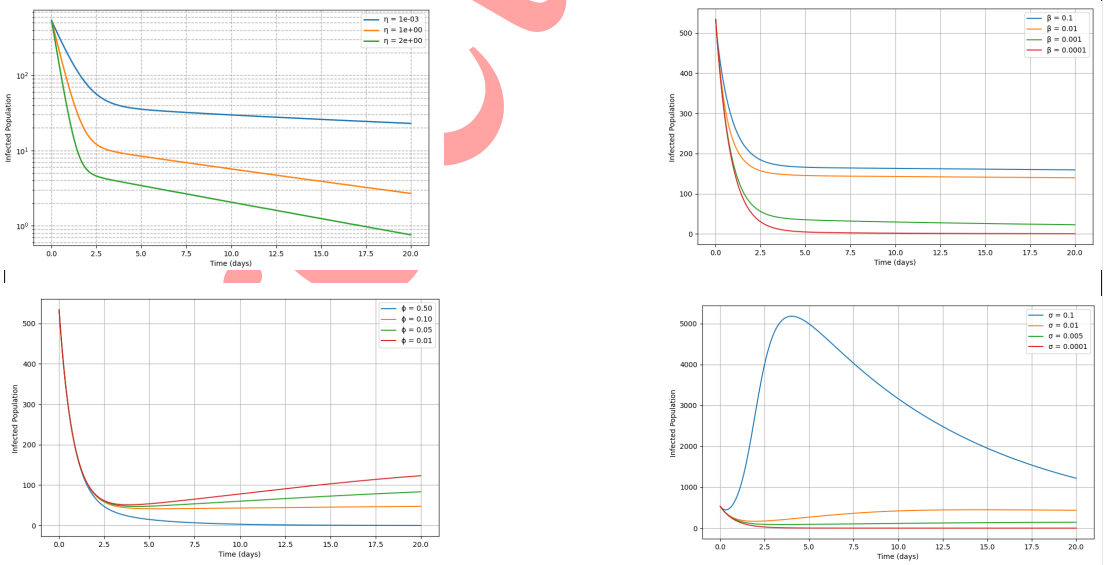

Figure 6: Behavior of the infected population for different values of η, β, ϕ, and σ.

5.5 Strategy 5: Mixed Strategy

This strategy combines vaccination, isolation, treatment, and awareness at relatively high levels. The control variables are set to $u_1 = 0.7$, $u_2 = 0.5$, $u_3 = 0.7$, and $u_4 = 0.7$.

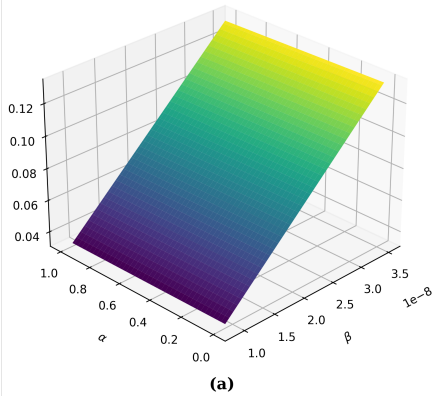

(a)

(a) Effect of β and α on $\mathcal{R}_0$

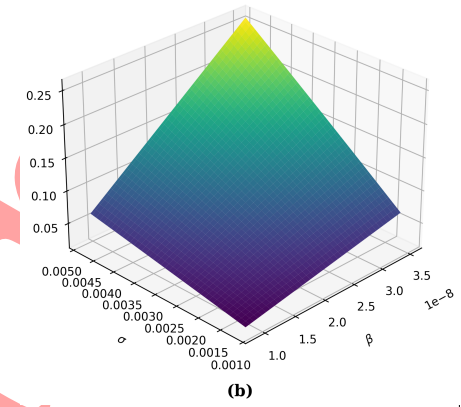

(b)

(b) Effect of β and σ on $\mathcal{R}_0$

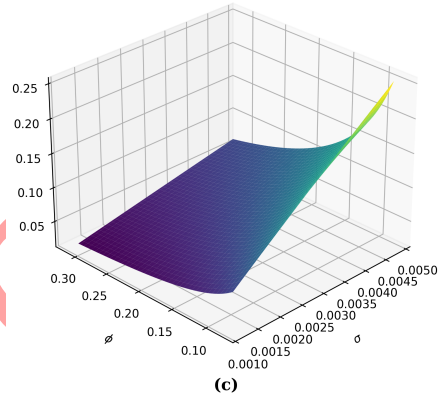

(c)

(c) Effect of σ and ϕ on $\mathcal{R}_0$

Figure 7: Illustration of the relationship between $\mathcal{R}_0$ and the key epidemiological parameters α, β, σ, and ϕ.

Figure 5 shows the result of the mixed intervention strategy. The susceptible population decreases sharply, the vaccinated population increases, and the infected population decreases more sharply than under any single-dominant strategy. The exposed population remains relatively small, while the recovered population continues to increase. The combination of vaccination, isolation-induced contact reduction, improved treatment, and increased public awareness was the most effective among the strategies considered.

The impact of key epidemiological parameters on the infected population is shown in Figure 6. The recovery rate η significantly accelerates the decline of infections: a larger η means a

faster transition from infected to recovered. The transmission parameter β critically determines epidemic severity: larger β raises the peak and extends the infection period, while smaller β reduces both. The parameter ϕ, which controls the flow from the exposed compartment back to the susceptible compartment, affects the replenishment of susceptibles and thereby prolongs transmission. The progression rate σ governs how quickly exposed individuals become infectious. In summary, the behavior of the epidemic model is highly sensitive to these key parameter values.

Figure 7(a) shows that higher levels of the infection rate β lead to greater $\mathcal{R}_0$, while increasing vaccine efficacy α reduces $\mathcal{R}_0$. Figure 7(b) shows the combined impact of β and σ: high β raises $\mathcal{R}_0$, while high σ (faster progression from exposed to infectious) yields smaller $\mathcal{R}_0$ in this parameterization. Figure 7(c) illustrates the inverse relationship between ϕ and $\mathcal{R}_0$, as also reflected in the sensitivity index in Table 3. These results contribute to understanding how key epidemiological variables influence disease spread and to identifying effective intervention strategies.

6 Conclusion

In this study, an extended mathematical model of chickenpox transmission was developed to evaluate the effects of vaccination, contact reduction through isolation, improved treatment, and public awareness. The numerical results demonstrated that increasing vaccination coverage and public awareness reduces the susceptible population and strengthens population-level immunity. These findings are supported by Foutel-Rodier et al. [19], who demonstrated the usefulness of mathematical models for evaluating vaccination-based intervention strategies and their effects on disease transmission. Previous studies of varicella have similarly shown that sufficient vaccination coverage can substantially reduce transmission [17, 45]. The present results also indicated that isolation and the associated reduction in contacts can decrease disease transmission, in agreement with Alshehri et al. [6], who showed that isolation-induced contact reduction restricts disease spread. However, the results suggest that isolation alone may not provide sufficient long-term control unless combined with treatment and public awareness measures. Improvements in treatment effectiveness and access to healthcare were shown to shorten the infectious period and reduce the disease burden, consistent with the findings reported in [44]. Among the intervention scenarios examined, the combined implementation of vaccination, isolation-induced contact reduction, improved treatment, and public awareness produced the greatest reduction in infections, emphasizing the importance of an integrated intervention strategy [9].

The effects of the individual interventions are explained directly by the structure of the model. Vaccination transfers individuals from H_S to H_V, reducing the population susceptible to infection. Isolation reduces transmission through the contact-modification factor $(1 - u_2)$. Improved treatment increases the effective recovery rate to $\eta + \kappa_3 u_3$, shortens the infectious period, and consequently reduces infection prevalence. Public awareness contributes through the awareness-induced vaccination term $\kappa_4 u_4$, which represents increased vaccine acceptance arising from improved risk perception. The combined strategy is therefore effective because it simultaneously reduces susceptibility and transmission, accelerates recovery, and promotes vaccination.

Limitations. The proposed model involves several simplifying assumptions. First, it does not capture all immunological features of varicella infection; immunity following chickenpox is generally long-lasting, whereas the return-to-susceptibility processes are represented by phenomenological parameters. Second, the epidemiological parameters are assumed constant, although contact frequency, vaccination uptake, treatment availability, and adherence to isolation may vary over time. Third, behavioral factors—including vaccine hesitancy, risk perception, and compliance with quarantine measures—are not explicitly modeled. Fourth, the model does not incorporate age structure, even though chickenpox transmission is strongly influenced by age-specific susceptibility and contact patterns, particularly among children aged 1–14 years. Finally, although Pontryagin's Maximum Principle provides the theoretical optimality conditions, the resulting optimal control system was not solved numerically using the forward-backward sweep method; the numerical experiments therefore use fixed representative control levels for scenario comparison rather than time-dependent optimal control trajectories.

Future Work. Future studies may extend the proposed framework by numerically solving the optimality system using the forward-backward sweep method to determine time-dependent optimal control trajectories. The model could also be improved by incorporating time-dependent epidemiological parameters, age structure, age-specific contact patterns, breakthrough infections following vaccination, and behavioral response functions describing vaccine hesitancy and adherence to isolation. Calibration and validation using observed chickenpox incidence and vaccination data would further improve predictive accuracy and practical applicability. Integrating economic costs into the objective functional would allow intervention strategies to be evaluated in terms of both epidemiological effectiveness and economic feasibility. Further developments could also investigate co-infections and the integration of data-driven or machine-learning methods for real-time epidemic prediction and intervention planning.

Declarations

Availability of Supporting Data

The data that support the findings of this study are available from the corresponding author upon reasonable request.

Funding

The author received no specific funding for this research.

Conflict of Interest

The author declares no known competing financial interests or personal relationships that could have influenced the work reported in this paper.

Artificial Intelligence Statement

Artificial intelligence-assisted tools were used solely to improve the language, readability, and organization of the manuscript. These tools were not used to generate the scientific results, perform the mathematical analysis, or draw the conclusions of the study. The author critically reviewed and verified all AI-assisted revisions and takes full responsibility for the accuracy, originality, and integrity of the final manuscript.

Publisher's Note

The publisher remains neutral regarding jurisdictional claims in published maps and institutional affiliations.

References

[1] Abiola, I. O., Oyewole, A. S., Yusuf, T. T. (2024). "Mathematical modelling of Lassa-fever transmission dynamics with optimal control of selected control measures". *Modeling Earth Systems and Environment*, 10(6), 7443–7458. https://doi.org/10.1007/s40808-024-02168-z

[2] Ahmad, W., Butt, A. I. K., Rafiq, M., Asif, Z., Ismaeel, T., Ahmad, N. (2024). "Modeling, analyzing and simulating the measles transmission dynamics through efficient computational optimal control technique". *The European Physical Journal Plus*, 139(7), 1–30. https://doi.org/10.1140/epjp/s13360-024-05368-9

[3] Akbari, R., Navaei, L., Shahriari, M. (2024). "Dynamical behaviour of fractional order SEIR mathematical model for infectious disease transmission". *Control and Optimiza-*

tion in Applied Mathematics, 9(1), 35–48. https://doi.org/10.30473/coam.2023.64849.1210

[4] Almuallem, N. A., Ali, H. M., Elsaid, E. M., Eid, M. R., Hassanin, W. S. (2025). "Mathematical simulation of optimal control measures to avoid chickenpox infection". *International Journal of Mathematics and Mathematical Sciences*, 2025(1), 3238188. https://doi.org/10.1155/ijmm/3238188

[5] Ali, A., Iqbal, Q., Asamoah, J. K. K., Islam, S. (2022). "Mathematical modeling for the transmission potential of Zika virus with optimal control strategies". *The European Physical Journal Plus*, 137(1), 146. https://doi.org/10.1140/epjp/s13360-022-02368-5

[6] Alshehri, A., Ullah, S. (2023). "Optimal control analysis of Monkeypox disease with the impact of environmental transmission". *AIMS Mathematics*, 8(7), 16926–16960. https://doi.org/10.3934/math.2023865

[7] Anderson, R. M., May, R. M. (1991). *Infectious Diseases of Humans: Dynamics and Control*. Oxford University Press, Oxford. https://doi.org/10.1093/oso/9780198545996.001.0001

[8] Baig, A., Zhouxin, L. (2025). "Modeling infectious diseases: From SIR models to diffusion-based approaches and numerical solutions". *arXiv preprint arXiv:2502.15439*. https://doi.org/10.48550/arXiv.2502.15439

[9] Baleanu, D., Hasanabadi, M., Mahmoudzadeh Vaziri, A., Jajarmi, A. (2023). "A new intervention strategy for an HIV/AIDS transmission by a general fractional modeling and an optimal control approach". *Chaos, Solitons & Fractals*, 167, 113078. https://doi.org/10.1016/j.chaos.2022.113078

[10] Barbieri, E., Cocchio, S., Furlan, P., Scamarcia, A., Cantarutti, L., Donà, D., Giaquinto, C., Baldo, V. (2024). "A population database analysis to estimate the varicella vaccine effectiveness in children <14 years in a high vaccination coverage area from 2004 to 2022". *Vaccine*, 42(26), 126387. https://doi.org/10.1016/j.vaccine.2024.126387

[11] Batista, M. (2021). "On the reproduction number in epidemics". *Journal of Biological Dynamics*, 15(1), 623–634. https://doi.org/10.1080/17513758.2021.2001584

[12] Behncke, H. (2000). "Optimal control of deterministic epidemics". *Optimal Control Applications and Methods*, 21(6), 269–285. https://doi.org/10.1002/oca.678

[13] Blayneh, K., Cao, Y., Kwon, H. D. (2009). "Optimal control of vector-borne diseases: Treatment and prevention". *Discrete and Continuous Dynamical Systems B*, 11(3), 587–611. https://doi.org/10.3934/dcdsb.2009.11.587

[14] Boulaaras, S., Yavuz, M., Alrashedi, Y., Bahramand, S., Jan, R. (2025). "Modeling the co-dynamics of vector-borne infections with the application of optimal control theory". *Discrete and Continuous Dynamical Systems – Series S*, 18(5), 1331–1352. https://doi.org/10.3934/dcdss.2024109

[15] Brauer, F., van den Driessche, P., Wu, J. (Eds.). (2008). *Mathematical Epidemiology*. Lecture Notes in Mathematics, Vol. 1945. Springer, Berlin. https://doi.org/10.1007/978-3-540-78911-6

[16] Brauer, F., Castillo-Chavez, C., Feng, Z. (2019). *Mathematical Models in Epidemiology*. Texts in Applied Mathematics, Vol. 69. Springer, New York. https://doi.org/10.1007/978-1-4939-9828-9

[17] Brisson, M., Edmunds, W. J., Gay, N. J., Law, B., De Serres, G. (2000). "Modelling the impact of immunization on the epidemiology of varicella zoster virus". *Epidemiology and Infection*, 125(3), 651–669. https://doi.org/10.1017/S0950268800004714

[18] Diekmann, O., Heesterbeek, J. A. P., Roberts, M. G. (2010). "The construction of next-generation matrices for compartmental epidemic models". *Journal of the Royal Society Interface*, 7(47), 873–885. https://doi.org/10.1098/rsif.2009.0386

[19] Foutel-Rodier, F., Charpentier, A., Guérin, H. (2025). "Optimal vaccination policy to prevent endemicity: A stochastic model". *Journal of Mathematical Biology*, 90(1), 10. https://doi.org/10.1007/s00285-024-02171-z

[20] Funk, S., Salathè, M., Jansen, V. A. A. (2010). "Modelling the influence of human behaviour on the spread of infectious diseases: A review". *Journal of the Royal Society Interface*, 7(50), 1247–1256. https://doi.org/10.1098/rsif.2010.0142

[21] Garnett, G. P., Grenfell, B. T. (1992). "The epidemiology of varicella–zoster virus infections: A mathematical model". *Epidemiology and Infection*, 108(3), 495–511. https://doi.org/10.1017/S0950268800050007

[22] Grassly, N. C., Fraser, C. (2008). "Mathematical models of infectious disease transmission". *Nature Reviews Microbiology*, 6(6), 477–487. https://doi.org/10.1038/nrmicro1845

[23] Hassan, A. H., Aldila, D., Noor Aziz, M. H. (2024). "Optimal control and stability analysis of monkeypox transmission dynamics with the impact of contaminated surfaces". *Frontiers in Applied Mathematics and Statistics*, 10, 1372579. https://doi.org/10.3389/fams.2024.1372579

[24] Heininger, U., Seward, J. F. (2006). "Varicella". *The Lancet*, 368(9544), 1365–1376. https://doi.org/10.1016/S0140-6736(06)69561-5

[25] Hethcote, H. W. (2000). "The mathematics of infectious diseases". *SIAM Review*, 42(4), 599–653. https://doi.org/10.1137/S0036144500371907

[26] Heydari Dastjerdi, R., Ahmadi, G., Dadkhah, M., Yari, A. (2023). "Optimal control of infectious diseases using artificial neural networks". *Control and Optimization in Applied Mathematics*, 8(2), 17–32. https://doi.org/10.30473/coam.2023.64776.1208

[27] Holmdahl, I., Buckee, C. (2020). "Wrong but useful—what COVID-19 epidemiologic models can and cannot tell us". *New England Journal of Medicine*, 383(4), 303–305. https://doi.org/10.1056/NEJMp2016822

[28] Jajarmi, A., Ebrahimzadeh, A., Khanduzi, R. (2025). "Coronavirus metamorphosis optimization algorithm and collocation method for optimal control problem in COVID-19 vaccination model". *Optimal Control Applications and Methods*, 46(1), 292–306. https://doi.org/10.1002/oca.3215

[29] Jose, S. A., Raja, R., Dianavinnarasi, J., Baleanu, D., Jirawattanapanit, A. (2023). "Mathematical modeling of chickenpox in Phuket: Efficacy of precautionary measures and bifurcation analysis". *Biomedical Signal Processing and Control*, 84, 104714. https://doi.org/10.1016/j.bspc.2023.104714

[30] Kalachev, L., Graham, J., Landguth, E. L. (2024). "A simple modification to the classical SIR model to estimate the proportion of under-reported infections using case studies in flu and COVID-19". *Infectious Disease Modelling*, 9(4), 1147–1162. https://doi.org/10.1016/j.idm.2024.06.002

[31] Kermack, W. O., McKendrick, A. G. (1927). "A contribution to the mathematical theory of epidemics". *Proceedings of the Royal Society of London, Series A*, 115(772), 700–721. https://doi.org/10.1098/rspa.1927.0118

[32] Khanduzi, R., Jajarmi, A., Ebrahimzadeh, A., Shahini, M. (2024). "A novel collocation method with a coronavirus optimization algorithm for the optimal control of COVID-19: A case study of Wuhan, China". *Computers in Biology and Medicine*, 178, 108680. https://doi.org/10.1016/j.compbiomed.2024.108680

[33] Kim, S., Choi, J. K., Suh, J., Park, S. H., Lee, J. (2024). "The epidemiologic and economic impact of varicella and herpes zoster vaccination in South Korea: A mathematical modelling study". *Vaccine*, 42(19), 4046–4055. https://doi.org/10.1016/j.vaccine.2024.05.016

[34] Lenhart, S., Workman, J. T. (2007). *Optimal Control Applied to Biological Models*. Chapman & Hall/CRC. https://doi.org/10.1201/9781420011418

[35] Li, T., Guo, Y. (2022). "Modeling and optimal control of mutated COVID-19 (Delta strain) with imperfect vaccination". *Chaos, Solitons & Fractals*, 156, 111825. https://doi.org/10.1016/j.chaos.2022.111825

[36] Nisar, K. S., Farman, M., Abdel-Aty, M., Ravichandran, C. (2024). "A review of fractional order epidemic models for life sciences problems: Past, present and future". *Alexandria Engineering Journal*, 95, 283–305. https://doi.org/10.1016/j.aej.2024.03.059

[37] Nkeki, C., Mbarie, I. (2025). "On a mathematical model and the efficacy of control measures on the transmission dynamics of chickenpox". *Bulletin of Biomathematics*, 3(1), 37–61. https://doi.org/10.59292/bulletinbiomath.1707079

[38] Omoloye, M. A., Adewale, S. O. (2021). "Optimal control analysis on mathematical model of dynamical transmission of Ebola–Malaria co-infections". *Journal of Information and Computational Science*, 11(9), 174–195.

[39] Ouakka, A., Alla Hamou, A., El Azzouzi, A., Agarwal, P. (2026). "A computational model of varicella dynamics with age-dependent waning immunity: Stability, parameter estimation, and optimal control via finite difference schemes". *Journal of Applied Mathematics and Computing*, 72(4), 152. https://doi.org/10.1007/s12190-026-02806-y

[40] Peter, O. J., Madubueze, C. E., Ojo, M. M., Oguntolu, F. A., Ayoola, T. A. (2023). "Modeling and optimal control of monkeypox with cost-effective strategies". *Modeling Earth Systems and Environment*, 9(2), 1989–2007. https://doi.org/10.1007/s40808-022-01607-z

[41] Shi, L., Lu, J., Sun, X., Li, Z., Zhang, L., Lu, Y., Yao, Y. (2023). "Impact of varicella immunization and public health and social measures on varicella incidence: Insights from surveillance data in Shanghai, 2013–2022". *Vaccines*, 11(11), 1674. https://doi.org/10.3390/vaccines11111674

[42] Siettos, C. I., Russo, L. (2013). "Mathematical modeling of infectious disease dynamics". *Virulence*, 4(4), 295–306. https://doi.org/10.4161/viru.24041

[43] Skrip, L. A., Townsend, J. P. (2019). "Modeling approaches toward understanding infectious disease transmission". In P. J. Krause, P. B. Kavathas, N. H. Ruddle (Eds.), *Immunoepidemiology* (pp. 227–243). Springer, Cham. https://doi.org/10.1007/978-3-030-25553-4_14

[44] Teklu, S. W. (2024). "Impacts of optimal control strategies on the HBV and COVID-19 co-epidemic spreading dynamics". *Scientific Reports*, 14, 5328. https://doi.org/10.1038/s41598-024-55111-8

[45] World Health Organization. (2014). "Varicella and herpes zoster vaccines: WHO position paper, June 2014". *Weekly Epidemiological Record*, 89(25), 265–288. https://www.who.int/publications/i/item/who-wer-8925-265-288

Authors' Bio-sketches

Author's Bio-sketch

Asiyeh Ebrahimzadeh is an Associate Professor in the Department of Mathematics Education at Farhangian University, Iran. She received her Ph.D. in Numerical Analysis from Iran University of Science and Technology. Her research interests include numerical analysis, optimal control, mathematical modeling, collocation methods, numerical optimization, and mathematics education. Her research particularly focuses on developing computational methods for solving applied optimal control problems and mathematical models arising in epidemiology, environmental systems, and other interdisciplinary applications. Corresponding author. Email: a.ebrahimzadeh@cfu.ac.ir